# QUANTIFICATION OF MURINE OLFACTORY RECEPTOR 691 AND 78 QUATERNARY STRUCTURE IN HEK293 CELLS USING SPATIAL INTENSITY DISTRIBUTION ANALYSIS

A thesis presented to the faculty of the Graduate School of Western Carolina University in partial fulfillment of the requirements for the degree of Master of Science in Biology

By

Danielle Nicole Voet

Director: Dr. Robert T. Youker
Associate Professor of Molecular Biology
Department of Biology

Committee Members: Dr. Amanda Storm, Biology,
Dr. Darby Harris, Biology

October 28th, 2022

# ACKNOWLEDGEMENTS

I would like to thank both of my parents for their constant support and encouragement while I have been in graduate school. Without their help I would not be where I am at and may not be crossing the finish line. More specifically, my mom has always been my greatest confidant and has never doubted my ability to succeed. My significant other, Truston Vorbeck, has always provided the necessary, and much needed laughter, to help me get through graduate school. Furthermore, my grandmother, Joyce Warren, has always been one of my biggest inspirations and fans.

It has been a privilege to attend Western Carolina University. Dr. Youker, my research advisor, has provided me with vast knowledge within the field of molecular biology. His guidance and support has not only guided me these past four years, but has also enabled me to encompass the skills necessary to excel and succeed going forward. Furthermore, my committee members, Dr. Amanda Storm and Dr. Darby Harris, have provided considerable support while I have been completing my thesis. I would also like to thank Dr. Jennifer Pluznick for the lucy-rho-flag 691 and 78 plasmids.\

TABLE OF CONTENTS

LIST OF TABLES

LIST OF FIGURES

# ABSTRACT

QUANTIFICATION OF MURINE OLFACTORY RECEPTOR 691 AND 78 QUATERNARY STRUCTURE IN HEK293 CELLS USING SPATIAL INTENSITY DISTRIBUTION ANALYSIS

Danielle Nicole Voet, M.S.

Western Carolina University (October 2022)

Director: Dr. Robert Youker

G-protein coupled receptors (GPCR) encompass a large number of protein receptors within the human genome. Because GPCRs are involved in numerous pathways including serotonin signaling in the brain, the receptors are often targets for drug development. Recent studies have demonstrated the presence of novel olfactory receptors (ORs), a member of the GPCR family, in the murine kidney but little is known about the function, and structure of these receptors. Spatial Intensity Distribution Analysis (SpIDA) has been used to measure the quaternary state (organization of receptor subunits) and surface density of GPCR proteins in live and fixed cells. In SpIDA, intensity histograms are generated and mathematically fitted from the cell images to obtain the quantal brightness (QB) of the receptor. This receptor QB can be compared to the QB of control proteins that are known to be monomer, or larger oligomers, therefore determining the quaternary, or oligomeric state of the receptor. Olfactory receptors (ORs) are members of the GPCR protein family and are responsible for our sense of smell. Several research groups have recently shown that olfactory receptors are not only located in the olfactory organs of our noses, but also present in

many other organ systems including the renal system. Activation of the Olfr78 receptor can lead to various responses in the body, ranging from changes in blood pressure to preventing the proliferation of cancer cells. It was determined that short chain fatty acids (SCFAs) act as a potential ligand for both receptors. While less studied, Olfr691 demonstrates similar structures and reactions to SCFAs, inferring that these two receptors demonstrate similar functions. Both of these receptors were studied with and without the presence of butyric acid using SpIDA in attempts to gain knowledge pertaining to the structure-function relationship of these proteins.

By determining the structural context of these receptors, further investigation of the conformational changes construed by ligand binding can be deduced, alluding to binding affinity and specificity associated with these ORs. This enables them to be further studied as potential targets for drug therapies. Additionally, bioinformatic based approaches were employed to gain insight into the protein structure and evolutionary relationships of this receptor with other similar GPCRs.

# INTRODUCTION

## G-protein-Coupled Receptors (GPCRs)

G-protein-Coupled Receptors, also referred to as GPCRs, are one of the largest family of cell-surface receptors in eukaryotes (de Mendoza et al. 2014). They mediate responses triggered by a diverse array of molecules that include hormones and neurotransmitters (Calebiro et al. 2015). There are approximately 800 and 1,000 GPCRs are associated with humans and mice, respectively (Congreve et al. 2020, Poll et al. 2021). GPCRs can be classified into four family classes: A, B1, F and C (Figure 1). Each receptor class is associated with unique protein domains, but all classes contain the standard seven transmembrane domain (Figure 2). GPCR receptors begin with an extracellular amino terminus and end with an intracellular carboxyl terminus (Fredriksson et al. 2003). These “cylindrical-like” structures contain ligand binding sites that enable G proteins to relay cell information from the exterior of the plasma membrane to the cell interior (Figure 2).

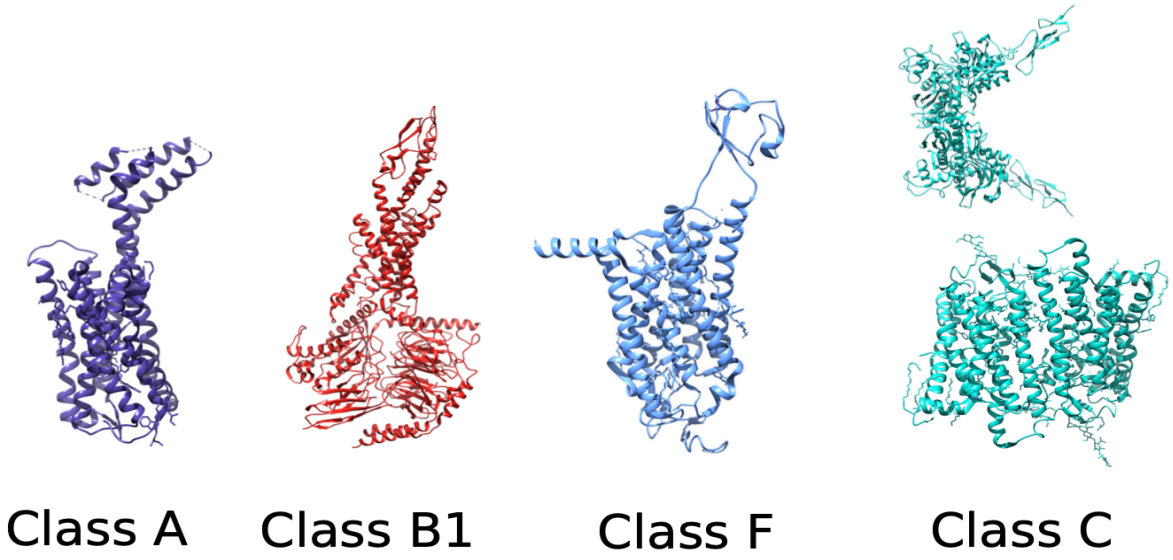


Figure 1: Representative crystal structures of GPCR family members. Structures generated using Chimera.

Crystal structure of class A (serotonin receptor, PBD: 6bqh), class B1 (glucagon receptor, PDB: 6lmk), class F (frizzled 4 receptor, PDB: 6bd4), and class C (extracellular domain from metabotropic glutamate receptor 3 (PDB: 2e4w) and 7TM from bovine rhodopsin (PDB: 1gzm) as a structural model to represent class because no full-length structures exist (modified from Youker and Voet 2019).

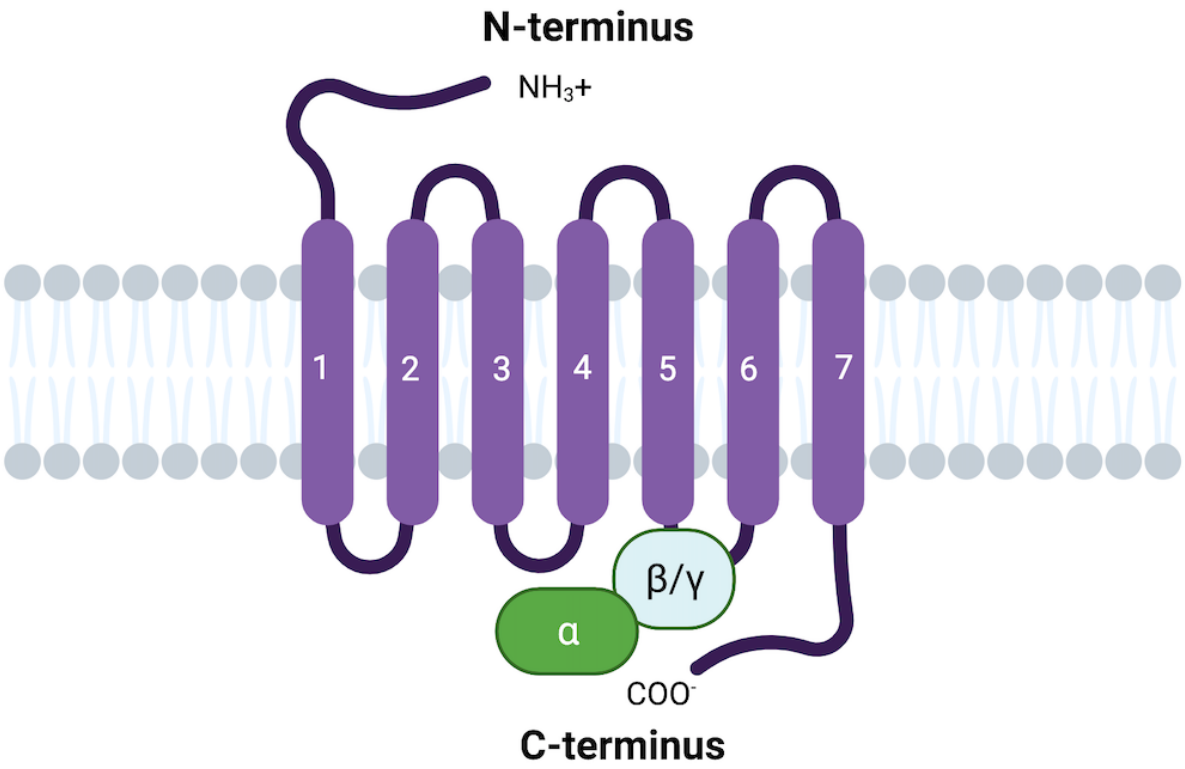


Figure 2: Schematic of G-Protein Coupled Receptor (GPCR). Image created in Biorender.

## G-Protein Coupled Receptors Signaling

Extracellular signaling within the GPCR family occurs when a ligand binds to a GPCR and the subsequent receptor undergoes a conformational change (Figure 3). Upon receptor activation, the trimeric G-protein complex dissociates into alpha (α-GDP) and beta (β)/gamma (γ) complex. Previously inactivated, the Gα subunit releases the bound Guanosine Diphosphate (GDP) acting as a guanine nucleotide exchange factor (GEF), enabling the GDP to be replaced with GTP (Guanosine-5'-triphosphate) (Harikumar, et al. 2007).

Oligomerization is a process that refers to the creation of higher order macromolecular complexes from protein monomers (Jenkins et al. 1996). Oligomeric structures of proteins might be larger in nature overall, yet the stability and genomic size of the given protein remain consistent (Hashimoto et al. 2010). Early studies suggested that activated GPCRs were only monomeric, but more recent studies have demonstrated that activated GPCRs can exist in higher order oligomeric states (for review see Gahbauer et al. 2016). Crystal structures of GPCRs have shed light onto some of the structural requirements needed for oligomerization (Gahbauer et al. 2016).

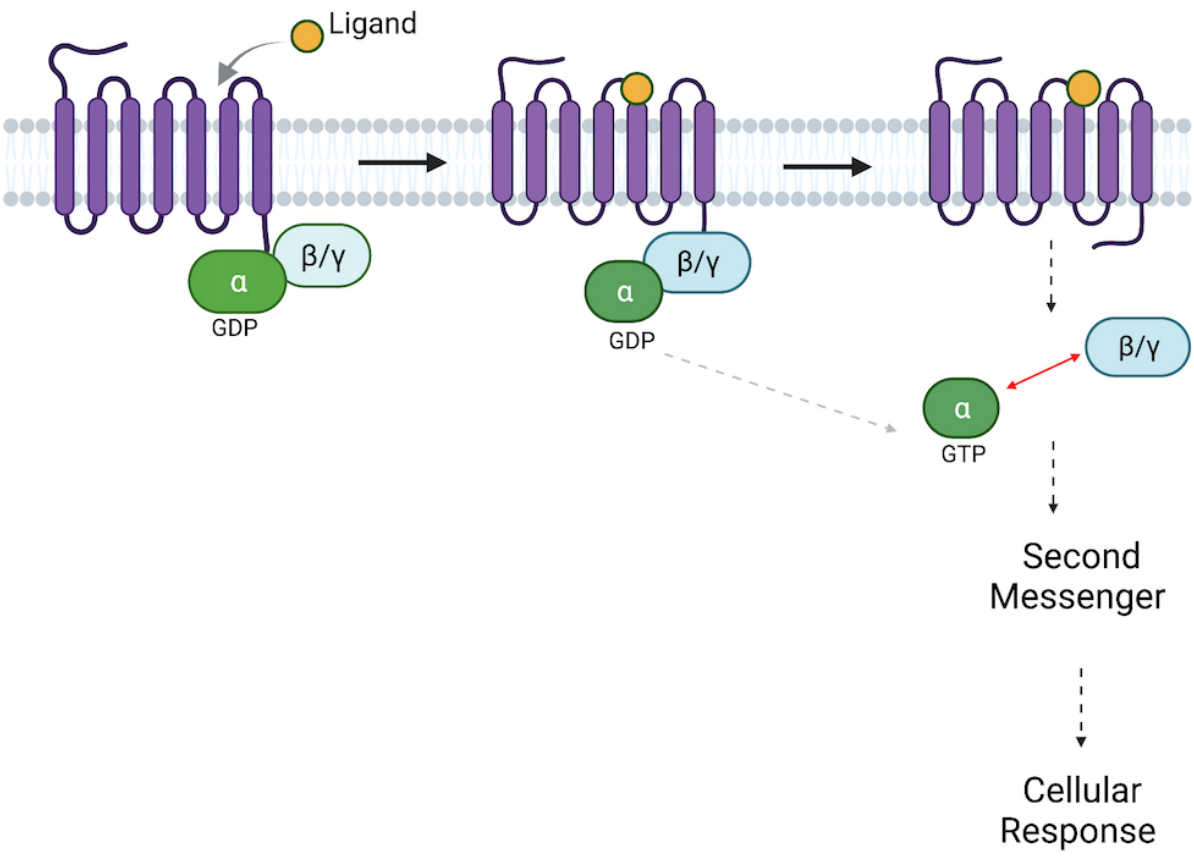


Figure 3: Schematic of GPCR Signaling activated by a canonical ligand. Image created in Biorender.

## Olfactory Receptors 78 & 691

Olfactory receptors were originally discovered in olfactory sensory neurons and epithelium cells that line the human airway. Olfactory receptors are members of the Class A rhodospin-like family of GPCRs (Figure 1A) (Natarajan et al. 2013). There are over 1,000 olfactory receptors in murine species and many olfactory receptors remain orphaned, with no known associated ligands (Natarajan et al. 2013). Olfactory receptor 78 (Olfr78) is expressed in the renal afferent arterioles in the mouse kidney and is involved in the secretion of renin and blood pressure regulation (Pluznick et al. 2013). Pluznick and colleagues observed that Olfr78 is responsive to short chain fatty acids (SCFAs), predominantly acetate and propionate, which are found as metabolites from gut microbiota (Pluznick et al. 2013).

While less is known about Olfactory receptor 691 (Olfr691), this receptor is deemed a novel renal receptor that contains known ligands, valerate and isovalerate (Rajkumar et al. 2014). Figure 3 depicts the predicted crystal structures associated with both Olfr78 and Olfr691 as determined by AlphaFold (Figure 3a and 3b, respectively).

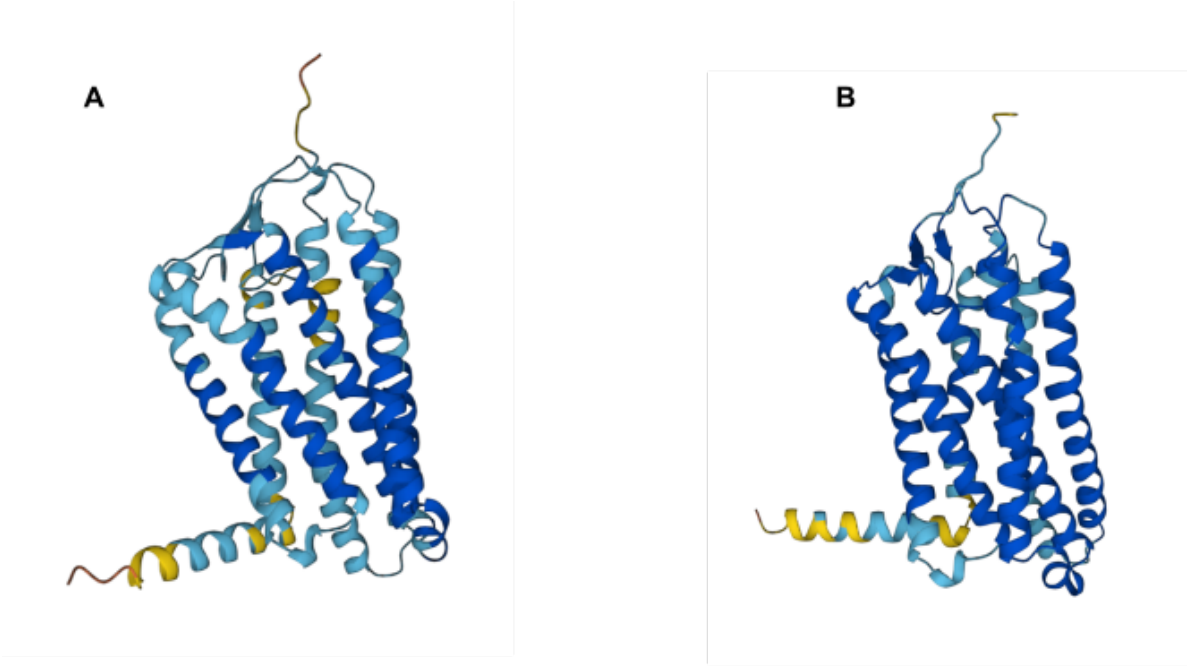


Figure 4: Crystal structure of olfactory receptor 691 and olfactory receptor 78. Images generated through AlphaFold.

A) AlphaFold structure of mouse olfactory receptor 51e2 (olfr78, UniProt Q8VBV9). Model is color coded for confidence with dark blue (very high pLDDT >90), light blue (confident 90 >pLDDT > 70), yellow (low 70 > pLDDT > 50), and orange (very low pLDDT < 50).

B) Predicted structure of olfactory receptor 691 (UniProt Q3MI58) generated from alpha fold. Model is color coded for confidence with dark blue (very high pLDDT >90), light blue (confident 90 >pLDDT > 70), yellow (low 70 > pLDDT > 50), and orange (very low pLDDT < 50).

Determining a structure-function relationship while characterizing both Olfr78 and Olfr691 novel renal receptors is ambitious in nature. The crystal structures predicted for these display similarities, with both receptors belonging to Class A GPCRs. Figure 4a represents Olfr78 (blue) and Olfr691 (purple) overlapped. Additionally, the BLAST sequence alignment demonstrated in Figure 4b displays a representation of both protein sequences aligned with one another, demonstrating marked similarities between Ollfr691 (top) and Olfr78 (bottom) (Figure 4b).

Alignment of the predicted crystal structures for Olfr-78 and Olfr-691 reveals marked differences in the predicted packing of the transmembrane domain and shape of the connecting loops between the alpha-helices (Figure 4A). This structural predication is somewhat surprising based on the BLASTP sequence alignment that clearly shows both proteins possess many identical amino acids in their transmembrane helices (Figure 4b).

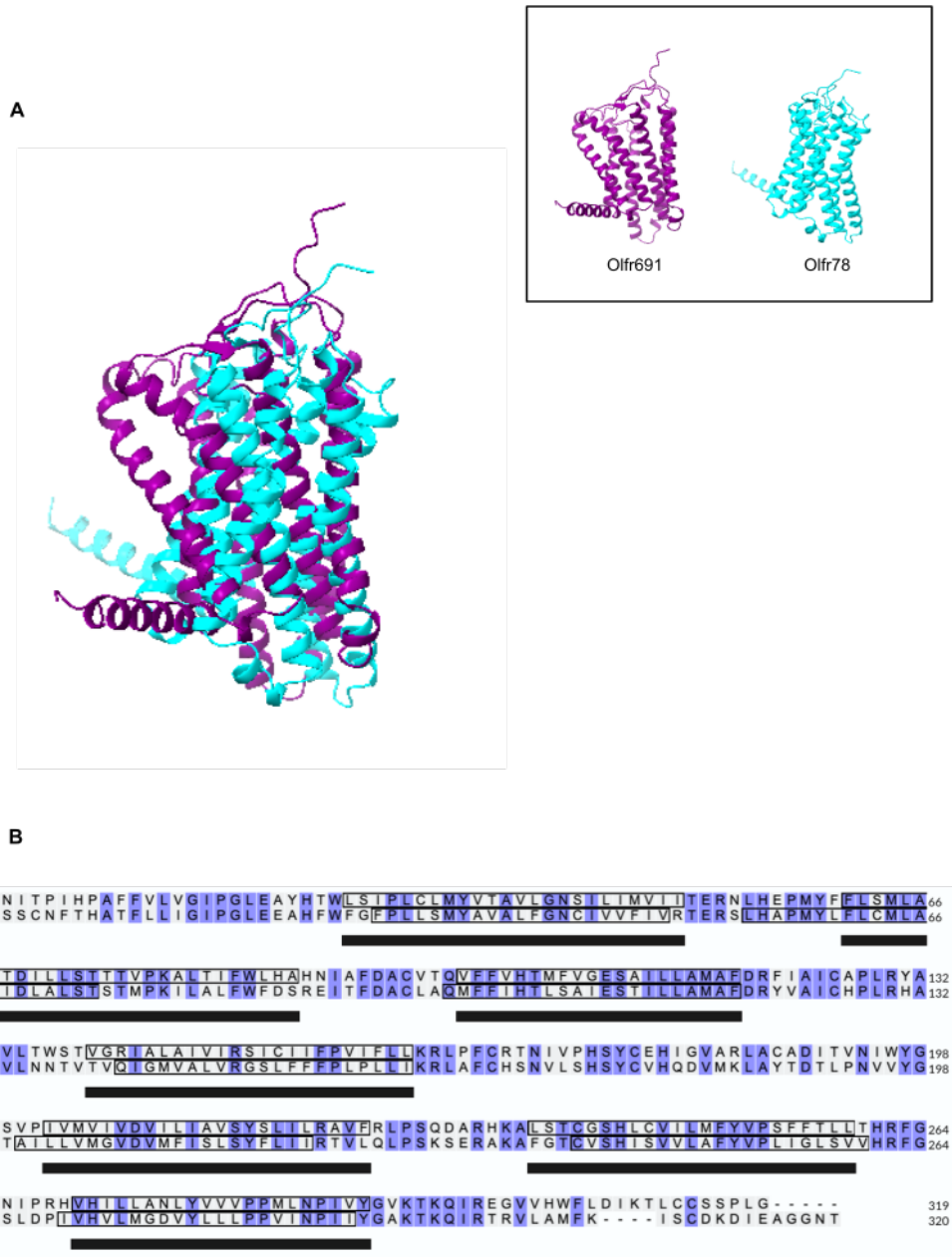


Figure 5: Olfactory receptor 78  and 691 comparison.

A) Predicted crystal structure of olfactory receptor 78 (cyan) and olfactory receptor 691 (magenta) aligned using matchmaker in Chimera.

B) Protein sequence alignment of Olfr691 and Olfr78. Sequence alignment generated through BLASTP. Blue indicates identical residues and outline denotes transmembranes.

## Fluorescent Fluctuation Techniques

Fluorescent fluctuation techniques (FFTs) are a suite of experimental approaches that can infer protein size/oligomeric status through analysis of the fluorescent signal emitted from the molecule (Youker and Voet 2020). The signal can be extracted from pixels of images taken using a confocal laser scanning microscope (CLSM), or from stationary spot measurements. These techniques can be performed on purified proteins in cuvettes, or in live/fixed cells (Youker and Voet 2020). There are several important differences that distinguish FFTs from one another (see Table 1). Specifically, the capability to measure live or fixed cells 2) capability to measure heterogenous mixtures of oligomers, and 3) capability to measure oligomers in cell membranes (Godin et al. 2010).

Table 1: Comparison of commonly used fluorescent fluctuation techniques used to study GPCR oligomeric structures in cells, modified from Godin et al. 2010.

| Technique | Samples | Mixture | Membrane |
|---|---|---|---|
| **FCS** | Live | No | No |
| **PCH** | Live | Yes | No |
| **RICS** | Live | No | Yes |
| **N&B** | Live | No | Yes |
| **SpIDA** | Live & Fixed | Yes | Yes |

Several of the most common forms of FFTs are fluorescence correlation spectroscopy (FCS), photon counting histograms (PCH), raster image correlation spectroscopy (RICS) and number and brightness (N&B) analysis. While each of these techniques are well-founded and robust, their limitations signify the importance of the development of spatial intensity distribution analysis (SpIDA). As shown in Table 1, FCS, PCH, RICS and N&B are only applicable to live cell samples, whereas SpIDA is the only FFT capable of being applied to fixed cells. An extension of SpIDA called fluorescence intensity fluctuation (FIF) analysis allows for deconvolution of complex mixtures of oligomers but is a more complicated analysis (Stoneman 2019).

## Spatial Intensity Distribution Analysis

Spatial intensity distribution analysis (SpIDA) is a recent analytical technique in fluorescent microscopy (Godin et al. 2010). Importantly, SpIDA enables the measurement of oligomeric GPCR species size and expression levels (Milligan et al. 2018). This technique employs mechanisms like photon counting histogram (PCH), a fluorescent fluctuation method that enables the characterization and brightness of fluorescent samples (Huang et al. 2004). This FFT implements Poissonian distributions to intensity histograms (Godin et al. 2010). With the use of CLSMs, these intensity histograms capture images of cells, either live or fixed, measuring the number of fluorescent molecules and their quantal brightness (Godin et al. 2010). There are several controls that must be employed to calibrate the microscope system before employing SpIDA. For example, Figure 5a refers to a fluorescent slide that is imaged at increasing laser intensities (0%, 3%, 12.5%, 25%, 100% outputs) to generate a plot of the variance versus intensity from the captured images. This enables the slope

(variance/intensity) to be calculated and this value is needed during the SpiDA calculation to compensate for detector noise.

Once the cells are properly imaged with the CLSM then fluorescent beads are imaged and used to determine the CLSM laser beam width (Figure 5b). Weissman and colleagues have developed a stand-alone program for SpIDA analysis that is free to use by the research community (https://neurophotonics.ca/software). Example screenshots for the running of the program are shown in Figure 6. While the comparison of SpIDA with other FFTs is still a topic of discussion, the benefits of this technique pose superior qualities, primarily the ability to study the expression and oligomeric states of both live and fixed cells (Table 1). Furthermore, the current use of SpIDA has proven beneficial when studying ligand interactions and shifts in oligomeric states in GPCRs due to conformational changes (Ward et al. 2017).

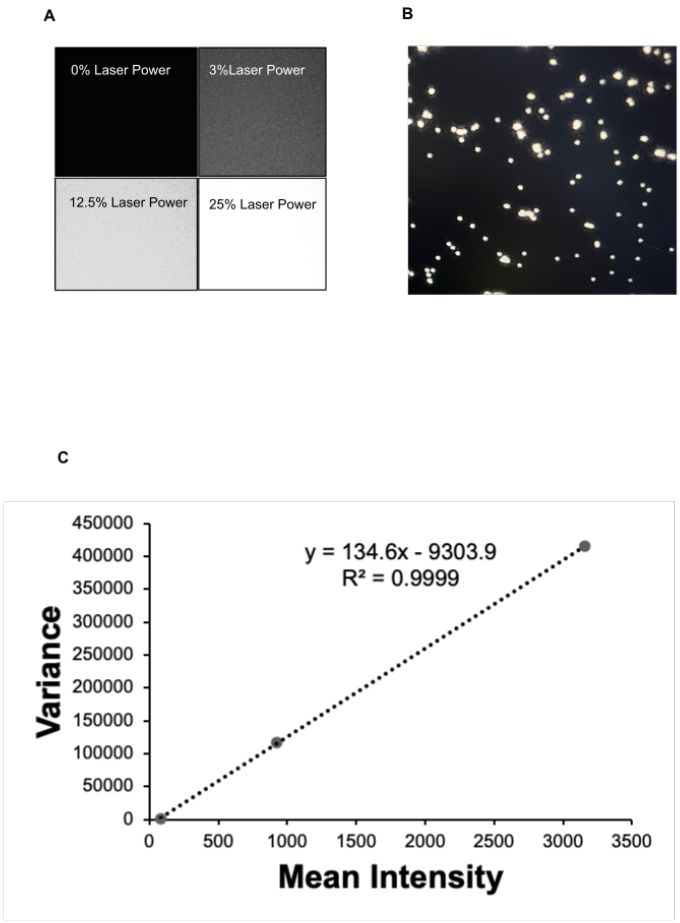


Figure 6: Calibrations for SpIDA.

A) Laser powers used were 0%, 3%, 12.5%, 25% for Nikon TE2000 CLSM

B) Image of orange-fluorescent beads (0.150 micron) taken with Nikon TE2000 CLSM

C) Plot of variance versus mean intensity including the fitted line with the $R^2$ and line equation displaying slope value needed for calibration during SpIDA analysis.

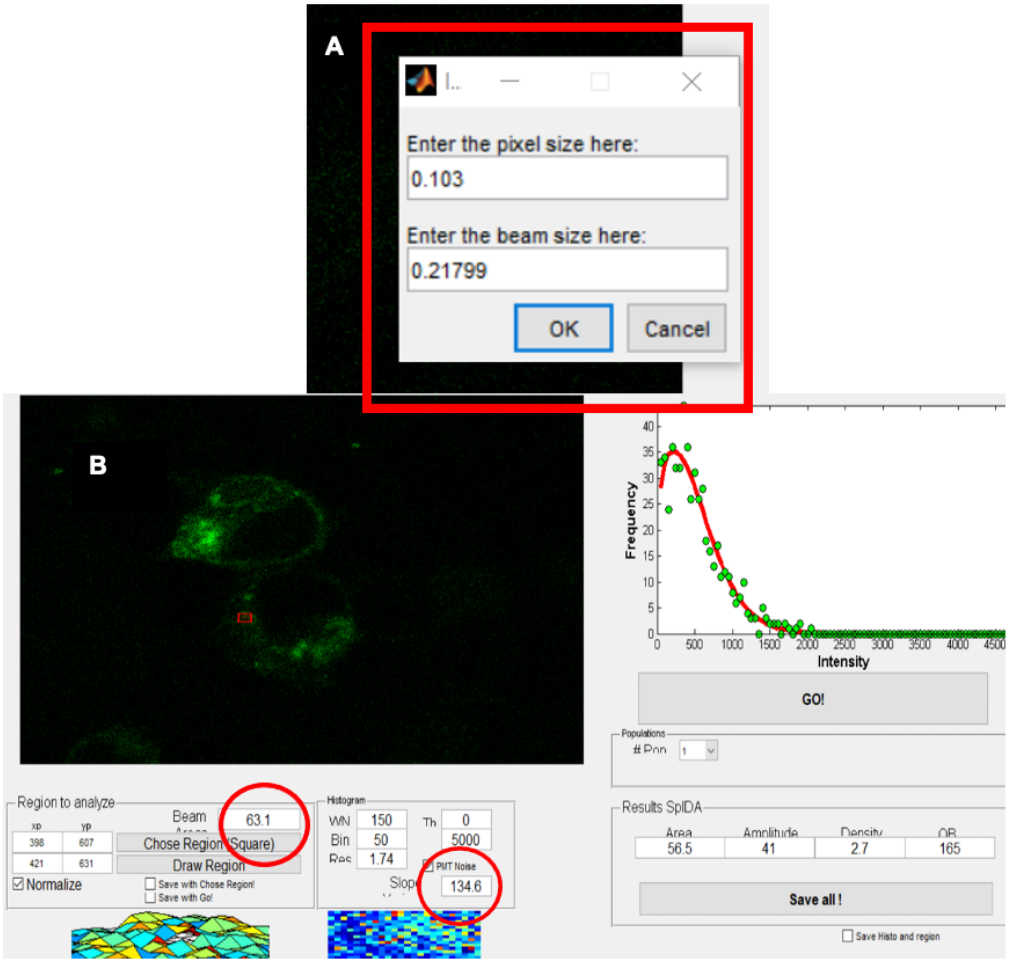


Figure 7: Example SpIDA analysis results using GUI_SpIDA software.

A) Example window in program for entering laser beam width and image pixel size. Both parameters are needed for the program to calculate the beam area when selecting a region of interest (ROI) and to calculate the receptor density in ROI.

B) Example window in program displaying the intensity histogram generated from the inputted Beam Area (ROI) and Slope Variance (134.6).

# MATERIALS AND METHODS

## Bacterial transformation of olfactory plasmids

Competent *Escherichia coli* (*E. coli*) DH5a cultures located in a -80º-C freezer were thawed out. Next, 2µl of Olfr691 or 78 plasmid DNA were added to the cells and incubated on ice for 10 minutes. These cells were then heat shocked at 42º-C for 45 seconds. Once this heat shock was completed, 500µl of Lysogeny broth (LB) was added and the contents of the tube were placed into 37ºC shaker set at 200rpm for one hour. Next, the solutions were streaked onto an LB-Ampicillin agar plate because OLFR691/78 contains the antibiotic resistance gene for ampicillin. These plates were wrapped with parafilm and placed into a 37º-C incubator overnight. The final product of transformation is the presence of white colonies on the LB-Ampicillin agar plate that contain the desired DNA.

## Purification of olfactory receptor plasmids

One transformed colony was picked and added to 2ml LB containing 50 mg/ml ampicillin. These tubes were then placed into a 37ºC shaker set to 200rpm overnight. Purification of the OLFR691 plasmid DNA was performed using the Thermofisher GeneJET Plasmid Midiprep Kit according to manufacturer's instructions. Plasmid concentration was measured using an NanoDrop 2000 and was 1,022.4 ng/µl.

## Culturing of HEK293 Cells

Human embryonic kidney (HEK) 293 cells were grown in Dulbecco's modified eagle medium (DMEM) supplemented with 10% fetal bovine serum (FBS) (Foundation grade, Gemini Bio). Spent growth media from stock plates was removed and discarded into a waste container containing 10% bleach. Next, 5ml of the recombinant enzyme

TrypLE was added to the stock plate to dissociate the growing HEK293 cells. The cells were then immediately placed into a 37º C incubator for 5 minutes. After this incubation period, 5ml of pre-warmed growth media was added to the stock plate containing TrypLE. This combined 10ml of media was then placed into a 15ml centrifuge tube and centrifuged at 800rpm for 5 minutes. After centrifugation, a pellet was formed at the bottom of the centrifuge tube. All media was removed from the centrifuge tube without disturbing the pellet. Next, the pellet was resuspended in 10ml of fresh growth media. The cells were counted, after being adequately resuspended, using a hemocytometer. For cell counting, 10µl of the resuspended cells were combined with 10µl of 0.4% Trypan blue dye to enable visualization of the viable cells. This combined 20µl was carefully pipetted onto a hemocytometer. The cells were counted in a total of four 16 square grid, these values were averaged together and multiplied by 20,000 to provide the approximate number of cells per milliliter. This value was multiplied by two (dilution factor) and divided by the number of desired cells per well (135,000) to provide the total amount of cells in milliliters to be added to each well of the 6 well plate.

**Transfection of HEK293 cells**

HEK293 cells were transfected with Olfr691 orOlfr78 plasmid using either FUGENE (Roche) or Continuum (Gemini Bio) lipid transfection reagent. For each transfection reaction, 75µl of Opti-MEM and 2µl of the lipid transfection reagent were combined and incubated for 5 minutes. In a second tube, 500ng of Olfr691 or Olfr78 plasmid DNA diluted into 75µl of Opti-MEM was combined with the Opti-MEM containing lipid. Once combined, they were incubated at room temperature for

approximately 45 minutes. Next, the mixture was carefully dropped over the cells and placed back into the 37 º C incubator for one to two days.

**Immunofluorescence**

Standard immunofluorescence protocol was followed using the Abcam immunocytochemistry and immunofluorescence protocol minus the antigen retrieval step and using 4% formaldehyde fixation. (https://www.abcam.com/protocols/immunocytochemistry-immunofluorescence-protocol). Briefly, the media from the cells was removed and washed with a pre-warmed phosphate-buffered saline (PBS) with a pH of 7.4. Once the cells were rinsed, the PBS was removed and 1mL of 4% paraformaldehyde in PBS was added to each well of the 6 well plate and placed in the 37º-C incubator for 10 minutes. Following incubation, the paraformaldehyde was removed, and each well was rinsed 3 times with cold PBS. Next, cells were permeabilized with PBS containing 0.1% Triton X – 100 for 10 minutes. The cells were then washed three times with PBS for five minutes per wash. Following permeabilization, cells were incubated with PBS containing 1% bovine serum albumin (BSA) and 22.52 mg/mL glycine in PBS with 0.1% Tween 20 (PBST) for 30 minutes at room temperature to block non-specific binding during subsequent antibody incubations.

For the antibody incubation chamber, A piece of filter paper soaked in PBS was placed in the center of a ~6-inch round Tupperware container with a sheet of parafilm placed on top of the filter paper. PBS-soaked Kim-wipes were lined along the edges of the container to keep the slides moist during the incubation period. The primary antibody, Monoclonal ANTI-FLAG M2 antibody produced in mouse (Sigma), was combined with 1% BSA and PBST in a 1:200 dilution. Next, 60µl of this primary

antibody dilution was pipetted onto the parafilm in the container then the coverslips were placed cell side down onto the diluted antibody. The container containing the coverslips was sealed and placed into a 4ºC fridge overnight. The following day, the coverslips were placed back into the 6 well plate containing fresh PBS. They were washed 3 times for five minutes per wash. The secondary antibody, AlexaFluor 546 goat anti-mouse (ThermoFisher), was combined with 1% BSA and PBST in a 1:500 dilution. Using the same container for incubation that contained a new sheet of parafilm, 60µl of this secondary diluted antibody was pipetted onto the parafilm in the container. The coverslips were removed from the six well plate and placed directly onto the secondary antibody solution cell side down in the container. This was incubated for one hour at room temperature in the dark. Once this incubation period was complete, the coverslips were removed from the container and placed back into the 6 well plates and washed three times with PBS for five minutes each wash. After these washes were complete, the coverslips were mounted onto glass slides to be used for analysis. The glass slides were wiped down with Kimwipes and appropriately labeled, then a small drop of VECTASHIELD Antifade Mounting Medium was added to the slide. The coverslips were then placed directly on top of the mounting medium cell side down. A small portion of nail polish was used to seal the outer edges of the coverslip. Next, the labeled glass slides with coverslips were placed into a 4ºC fridge until they were ready to be analyzed.

**Nikon TE2000 Confocal Microscope**

The Nikon TE2000 confocal laser scanning microscope was used to analyze stained cells. A 543-nm laser was used to excite the samples. The pixel dwell time used

was 9.36μs and the images were taken with 1024 pixels per line and 1024 lines per frame (1024x1024). The detector was set at 590/50 and the gain was 6.8V. The field zoom was set to 106.0μm and each sample imaged was captured using a 12.5% laser power. Additionally, blank fluorescent microscope slides were imaged at each laser (no laser, 3% laser, 12.5% laser, 25% laser and 100% laser power) power to provide the necessary data to determine the slope variance used for SpIDA analysis. Lastly, a Z-stack of 633nm fluorescent beads were imaged with 3% or 12.5% laser power, a zoom of 3.38 and a 6.8 gain to acquire the data necessary to calculate the beam waist area.

**Spatial Intensity Distribution Analysis (SpIDA)**

Each image obtained from the confocal laser scanning microscope was saved and converted to .TIFF files using Fiji (Fiji is Just Image J). The beam waist radius used was 0.2179μm$^2$. This value was calculated by dividing the FWHM by 2 to obtain the radius, then multiplying the square of this value by 3.14. Below is the calculation used to obtain the beam waist radius:

Waist Radius:

Average FWHM = 0.5277μm

0.5277μm/2 = 0.26358μm (this equals the radius)

Then, the area was determined by $\pi(0.26358\mu m)^2$ which equals 0.21787μm$^2$

These calculations follow the protocols used by Milligan et al. 2015. ROIs were maintained between 54.8 – 66.9 beam areas throughout analysis with the SpIDA software, with the average ROI being 61 beam areas. The pixel size was 0.103μm. The

slope variance was determined by graphing the mean intensity versus variance and determining the slope of this equation. The first experiment consisted of slope variances of 134.6 (corresponding to Set I, consisting of a pixel dwell time of 9.36μs) and 149.77 (for Set II, consisting of a pixel dwell time of 5.04μs). Once the analysis of this experiment was completed, a pixel dwell time of 9.36 was used for all experiments going forward. For experiment 2, a slope variance of 259.71 was calculated. For experiment 3, the calibration slides were saturated providing a negative slope value. Because of this, a value of 197.155 was used as the slope variance, obtained by averaging the values from the first two experiments. Once these values are inputted into the SpIDA software and a ROI is chosen then an Intensity versus Frequency graph is generated and fitted. Amplitude, density, and quantal brightness are extracted from this fitted plot. The average quantal brightness per cell is then graphed against the average density per cell. Raw quantal brightness values are divided by the average background quantal brightness to determine the oligomeric status of the receptor. Normalized quantal brightness (termed monomeric equivalent unit = MEU) values that were greater than 1.5 standard deviations above the average value were considered dimers/higher-order oligomers.

**Bioinformatics**

AlphaFold was used to predict the protein structures for Olfr78 (UniProt: Q8VBV9) and Olfr691 (UniProt: Q3MI58). The structures were predicted from the amino acid sequences of the given protein and per-residue confidence scores (pLDDTs) were generated, with scores about 50 being considered structurally accurate when using this system. With these predicted structures, ConSurf was then used to identify regions of

conservation between amino acids to indicate any potential protein-protein interactions. Default settings were used when using this server. Both sequences were aligned through BLASTP to visually denote regions of similarities between these sequences. Default settings were used when using BLASTP. Furthermore, the crystal structures of both proteins were overlapped with ChimeraX-1.4 software based on their associated PDB files.

## Statistics

The raw sets of data were collected from GUI_SpIDA and normalized to their background QB values or their 2º Ab only QB values, both acting as controls. These raw values were averaged and the QB values for the proteins for the given experiment were divided by this value, providing their normalized values, expressed in terms of monomeric equivalent units (MEUs). To decipher whether the cells were potential dimers or higher order oligomers, the standard deviation of the averaged QB of the controls was taken and subsequently multiplied by 2, setting the cutoff between monomers and dimers/higher order oligomers.

Three undergraduate students analyzed Olfr78 and Olfr691 images with GUI_SpIDA to compare the robustness of the analysis workflow. Undergraduate student QB and receptor density data were compared to Danielle Voet's (D.V.) results. A two tailed t-test or a Kruskal-Wallis test were implemented for the comparison of QB and density values. Two tailed t-tests were used for experiments pertaining to Olfr78 and Olfr691 data, and the Kruskal-Wallis test was used for data for the Olfr691 + butyric acid. The significance level of 0.05 was used as alpha for both tests.

# RESULTS

## Olfactory Receptor 691 oligomeric status

HEK293 cells were transfected with Lucy-Rho tagged Olfr-691 (Figure 7a). The Lucy-Rho tag improves the assembly and trafficking of olfactory receptors without altering receptor signaling at the plasma membrane (Shepard et al. 2013). The oligomeric status of Olfr-691 in fixed cells was determined using SpIDA. Thirty-seven cells from two experiments were used for measurements. Eleven cells with 2º Antibody (Ab) only staining was measured as a control (Figure 7b). Three to four regions of interest (ROIs) per cell were used in the calculations for a grand total of 135 ROIs (Figure 7b). These sets of values were normalized against the images captured of the background outside the cell, or the measurements of the 2º Ab only cells (Figure 7c&d). Olfr-691 was present as mostly monomers and species ranging in size between monomer and dimer (94.7%). A small percentage of the receptor was dimer or higher order oligomers (5.3%) (Figure 7e).

A

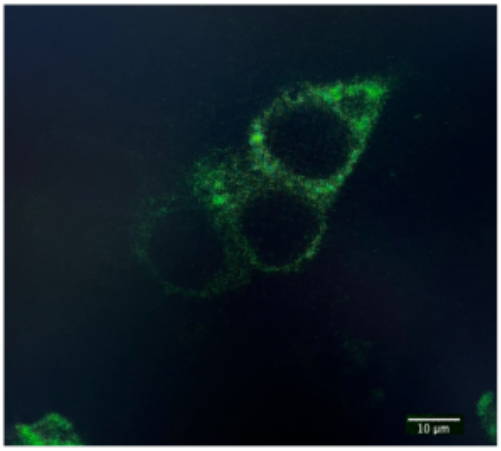
10 µm

B

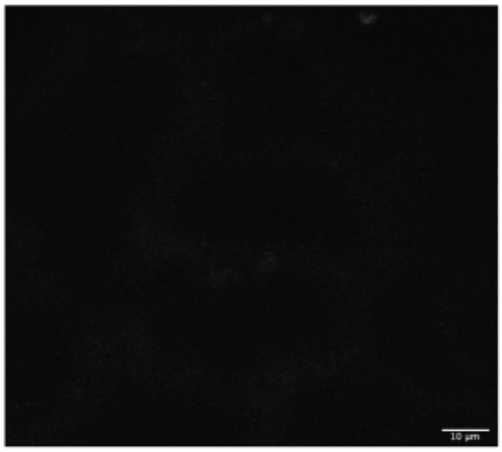
10 µm

C

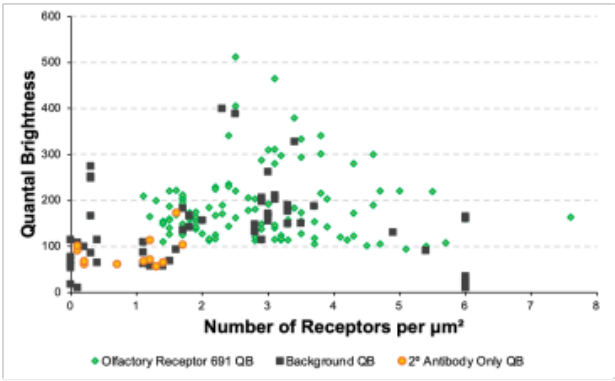
Quantal Brightness
Number of Receptors per µm²
Olfactory Receptor 691 QB
Background QB
2° Antibody Only QB

D

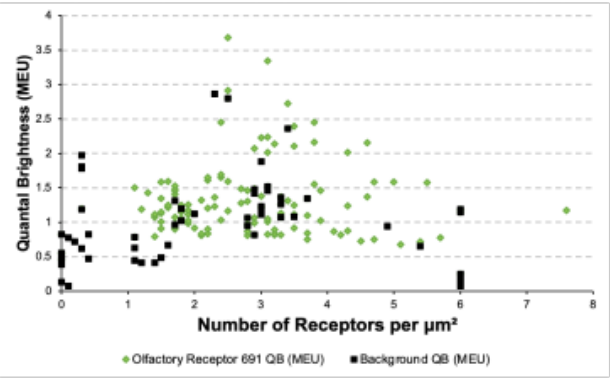
Quantal Brightness (MEU)
Number of Receptors per µm²
Olfactory Receptor 691 QB (MEU)
Background QB (MEU)

E

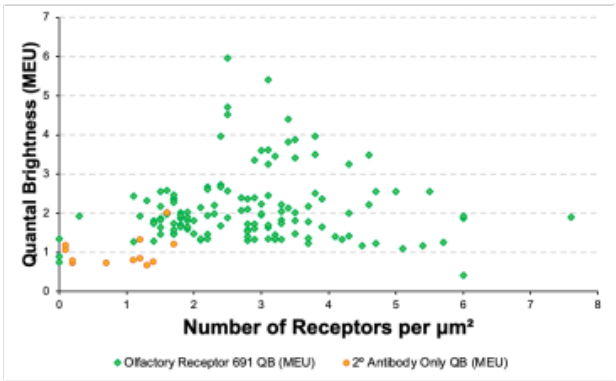
Quantal Brightness (MEU)
Number of Receptors per µm²
Olfactory Receptor 691 QB (MEU)
2° Antibody Only QB (MEU)

F

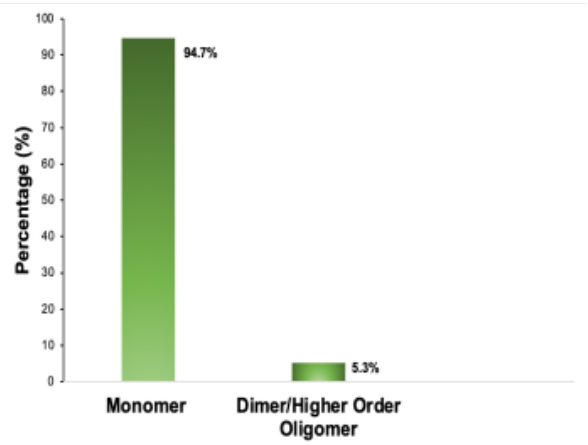
Percentage (%)
94.7%
5.3%
Monomer
Dimer/Higher Order Oligomer

Figure 8: Olfactory receptor 691 data.

A) Representative image of olfactory receptor 691

B) Representative image of slide treated with 2º Ab only

C) Raw QB versus receptors/μm² of olfr691, background and 2 º Ab only

D) Normalized QB versus receptors/μm² for olfr691 plotted with the background

E) Normalized QB versus receptors/μm² for olfr691 plotted with the 2 ºAb only

F) Bar graph representing percentages of monomers versus higher order oligomers

### Olfactory Receptor 691 with Butyric Acid

HEK293 cells expressing Lucy Rho-tagged Olfr-691 were incubated with 0.1 mM butyric acid for 30 minutes then cells were fixed for subsequent SpIDA analysis (Figure 8a). Three to four ROIs from twenty-four cells were measured for a grand total of 135 measurements. The distribution of oligomeric sizes was similar in the presence of 0.1 mM butyric acid compared to absence (Figure 7c & Figure 8c). The majority of Olfr691 appeared to be monomers (94.7%), with a small range being deemed dimers or higher order oligomers (5.3%) (Figure 8e).

A

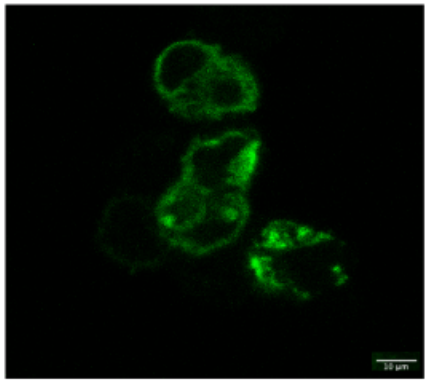

B

C

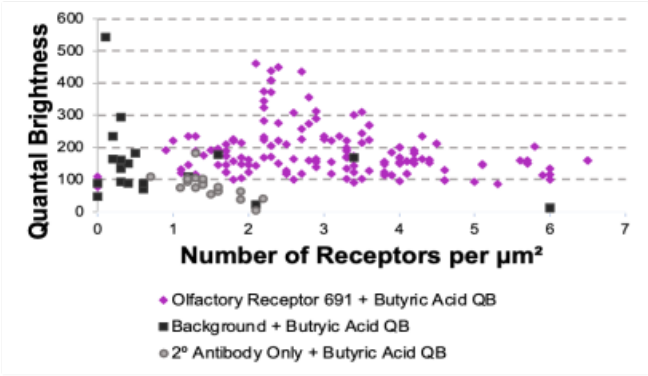
Quantal Brightness
600
500
400
300
200
100
0
0 1 2 3 4 5 6 7
Number of Receptors per µm²
Olfactory Receptor 691 + Butyric Acid QB
Background + Butryic Acid QB
2º Antibody Only + Butyric Acid QB

D

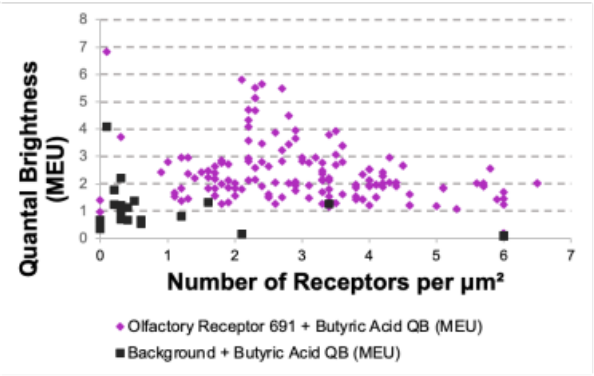
Quantal Brightness (MEU)
8
7
6
5
4
3
2
1
0
0 1 2 3 4 5 6 7
Number of Receptors per µm²
Olfactory Receptor 691 + Butyric Acid QB (MEU)
Background + Butyric Acid QB (MEU)

E

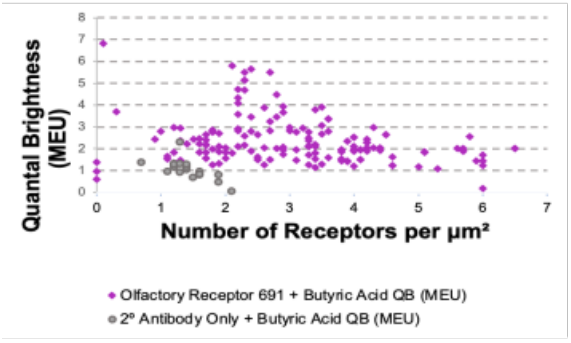
Quantal Brightness (MEU)
8
7
6
5
4
3
2
1
0
0 1 2 3 4 5 6 7
Number of Receptors per µm²
Olfactory Receptor 691 + Butyric Acid QB (MEU)
2º Antibody Only + Butyric Acid QB (MEU)

F

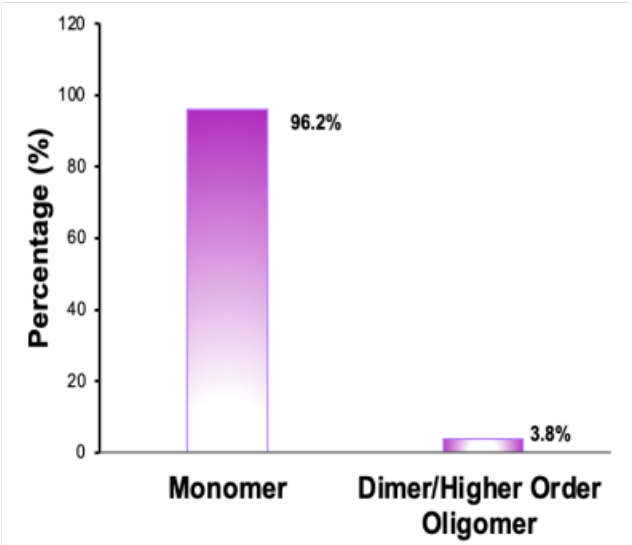
Percentage (%)
120
100
80
60
40
20
0
96.2%
3.8%
Monomer
Dimer/Higher Order Oligomer

Figure 9: Olfactory receptor 691 data with the addition of butyric acid

A) Representative image of olfactory receptor 691 with the addition of butyric acid

B) Representative image of slide treated with 2º Ab only with the addition of butyric acid

C) Raw QB versus receptors/μm² of olfr691, background and 2 º Ab only

D) Normalized QB versus receptors/μm² for olfr691 plotted with the background

E) Normalized QB versus receptors/μm² for olfr691 plotted with the 2 ºAb only

F) Bar graph representing percentages of monomers versus dimer/higher order oligomers

## Olfactory Receptor 78

The quantal brightness for Olfr-78 was used in one experiment and thirty-seven cells were imaged with the Nikon TE2000 confocal laser scanning microscope (Figure 9b). A total of 248 ROIs were analyzed for Olfr-78 and 54 ROIs were measured outside the cells. Olfr-78 was mostly monomeric in size with a large distribution of values between one and two (96.2%). The percentage of dimers and higher order oligomers was low (3.8%), similar to Olfr-691 in the absence or presence of butyric acid.

A

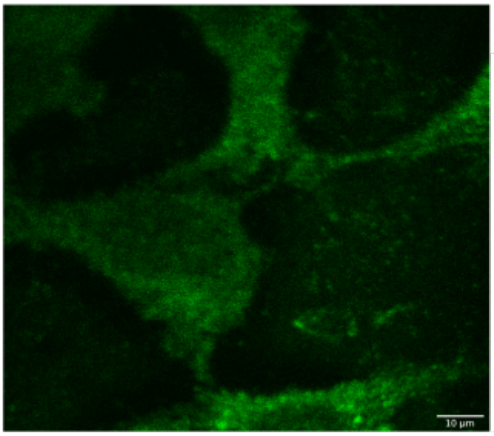
10 µm

B

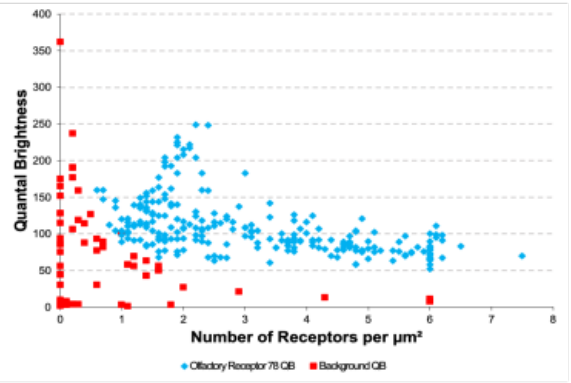
Quantal Brightness
Number of Receptors per µm²
Olfactory Receptor 78 QB
Background QB

C

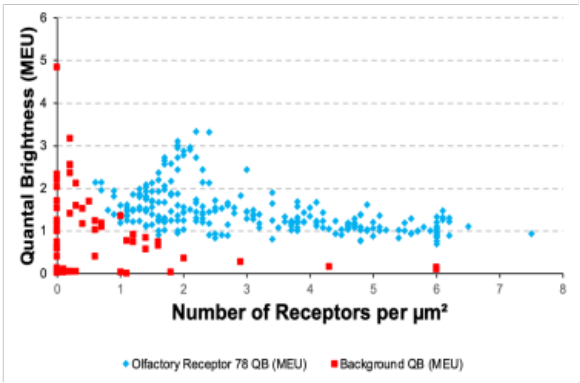
Quantal Brightness (MEU)
Number of Receptors per µm²
Olfactory Receptor 78 QB (MEU)
Background QB (MEU)

D

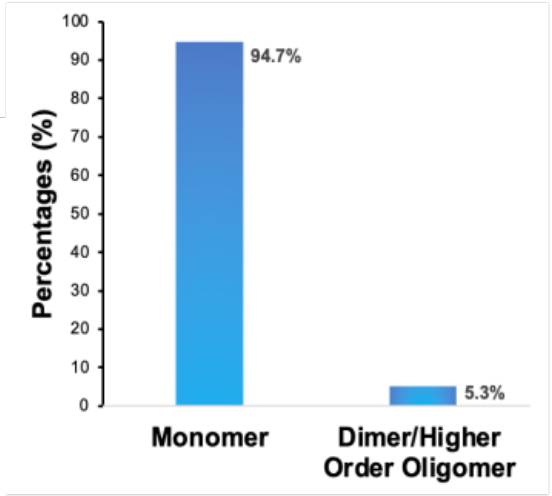
Percentages (%)
94.7%
5.3%
Monomer
Dimer/Higher Order Oligomer

Figure 10: Olfactory receptor 78 data with the addition of butyric acid.

A) Representative image of olfactory receptor 78
B) Raw QB versus receptors/μm² of olfr78 + background QB
C) Normalized QB versus receptors/μm² for olfr78+ plotted with the background
D) Bar graph representing percentages of monomers versus dimer/higher order oligomers

# DISCUSSION

GPCRs compose the largest family of cell-surface receptors, are widely studied due to their medical importance (Kobilka et al. 2007). Because of this, gaining a fundamental understanding of the structure-function relationship between GPCRs and associated ligands remains critical. Olfr-78 is expressed in the renal afferent arterioles and is activated by SCFAs (Pluznick et al. 2012). While acetate and propionate are dominant ligands for Olfr78, the SCFA butyrate was determined to weakly activate the receptor (Pluznick et al. 2012).

There is very little information on the structural organization of Olfr-78 and Olfr-691. Therefore, I employed SpIDA to determine the oligomeric state of both receptors in HEK293 cells. Normalized quantal brightness values ranged from one to six and most values measured between one to two subunits. These results were similar to previous SpIDA studies performed with the serotonin receptor Serotonin 5-Hydroxytryptamine 2C that is also a GPCR (Milligan et al. 2015). Since fractional receptors cannot exist, these SpIDA results suggest that both olfactory receptors exist as a mixture of monomers and dimers in the cell under basal conditions.

Addition of 0.1 mM butyric acid to Olfr-691 did not alter the oligomeric distribution of the receptor. This result was not unexpected given that previous research used 0.5mM, 5mM and 15mM of butyric acid concentrations and observed only weak activation (Rajkumar et al. 2014). Furthermore, acetate and propionate were demonstrated to be highly more potent ligands for both olfactory receptors (Pluznick et al. 2012).

Undergraduate students in Dr. Youker's lab analyzed the image data sets collected for Olfr-691 and Olfr-78 in parallel to determine the reliability and robustness of the SpIDA technique against user bias or due to differences in selection of ROIs. The quantal brightness recovered for Olfr78 and Olfr691 receptors were similar regardless of the researcher performing the analysis (Tables 2-4). Depicted in Table 2 is the comparison of Danielle Voet (D.V.) results to a Western Carolina University undergraduate student (student 1), illustrating the averages of the densities and quantal brightness for Olfr691 receptor. The average quantal brightness reported here was approximately 181.8, which was consistent with their overall average of 178.7. However, the densities vary by approximately 2.3 units, and this is most likely due to different ROIs selected by the individual researcher. These results also demonstrate that the oligomeric state of Olfr691 was constant over these concentration ranges. A two tailed t-test was performed for these sets of receptor's QB and density values. While the values for the Olfr691 QB were not statistically significant ($p>0.05$), the values for the densities were deemed statistically significant ($p< 0.05$). A Kruskal-Wallis test was applied for the QB and density values for Olfr691 in addition to butyric acid. The test demonstrated that the QB values among students was not statistically significant ($p>0.05$), while the values obtained for the density were deemed statistically significant ($p< 0.05$). While the density values are statistically significant, these results are demonstrative that a range in receptor concentration does not appear to affect oligomerization of Olfr691.

Table 2: Table depicting the average of quantal brightness and densities calculated with SpIDA for Olfr691.

| Olfactory 691 Receptor | Density | QB |
|---|---|---|
| **D.V.** | 2.78 | 181.76 |
| **Student 1** | 6.09 | 178.69 |

Table 3: Table depicting the average of quantal brightness and densities calculated with SpIDA for Olfr691 + butyric acid.

| Olfactory 691 Receptor + Butyric Acid | Density | QB |
|---|---|---|
| **D.V.** | 3.06 | 187.72 |
| **Student 1** | 8.92 | 164.46 |
| **Student 2** | 3.2 | 135.57 |

Student 3 was able to analyze the same images collected by the CLSM of the Olfr78 receptor with SpIDA, eliminating variation in experimental conditions. The density and quantal brightness averages obtained from both analyses were similar (Table 4). The consistent quantal brightness values obtained despite variations in ROIs size and slope variances suggests that under these circumstances there was no user bias, nor large impact from ROIs selected. A two tailed t-test was applied for the QB and density values between both students and both sets were not statistically significant ($p>0.05$).

Table 4: Table depicting the average of quantal brightness and densities calculated with SpIDA for Olfr78.

| Olfactory 78 Receptor | Density | QB |
|---|---|---|
| **D.V.** | 3.07 | 108.74 |
| **Student 3** | 3 | 139.349 |

These results suggest the average quaternary structure recovered by SpiDA under these experimental conditions is not influenced by the researcher conducting the analysis. Further research needs to be performed to determine if the oligomeric structure Olfr-78 and Olfr-691 receptor is similar in live cells. In addition, concentration series for the known SCFAs should be performed to determine if the quaternary structure of the receptors change with increasing ligand concentration.

A limitation to the present study is the inability to detect mixed hetero oligomers of the receptors. Olfr-691 and Olfr-78 could form oligomers with other receptors in the cell and/or endogenous versions of both olfactory receptors. In either case, these receptors are not labeled and are thus invisible to the SpIDA measurement. Thus, the average oligomeric size observed should be considered a lower estimate for these receptors.

The mechanism that mediates the observed oligomerization of Olfr-691 and 78 is not known. Amino acid interactions, lipid interactions, or both could be involved in this process. I performed ConSurf analysis to identify conserved amino acids on the surface of both receptors that might be involved in protein-protein interactions. Both receptors had patches of conserved amino acids on the surfaces of their predicted structures but there was very little overlap in the regions identified (Figure 12). Protein backbone alignment using the matchmaker plugin in ChimeraX revealed a 2.79 angstrom difference between the two receptor backbones and this difference was reduced to 1.00 angstroms if a small number of amino acids were pruned from the analysis (pruned to 261 amino acids). There were subtle differences in the loop regions and the predicted packing and orientation of the transmembrane regions (Figure 12c). More in-depth

computational analyses would be needed to investigate these conserved patches, such as molecular dynamic simulations and potential docking studies. Also, mutation of conserved surface residues could be employed to assess impact on receptor oligomerization.

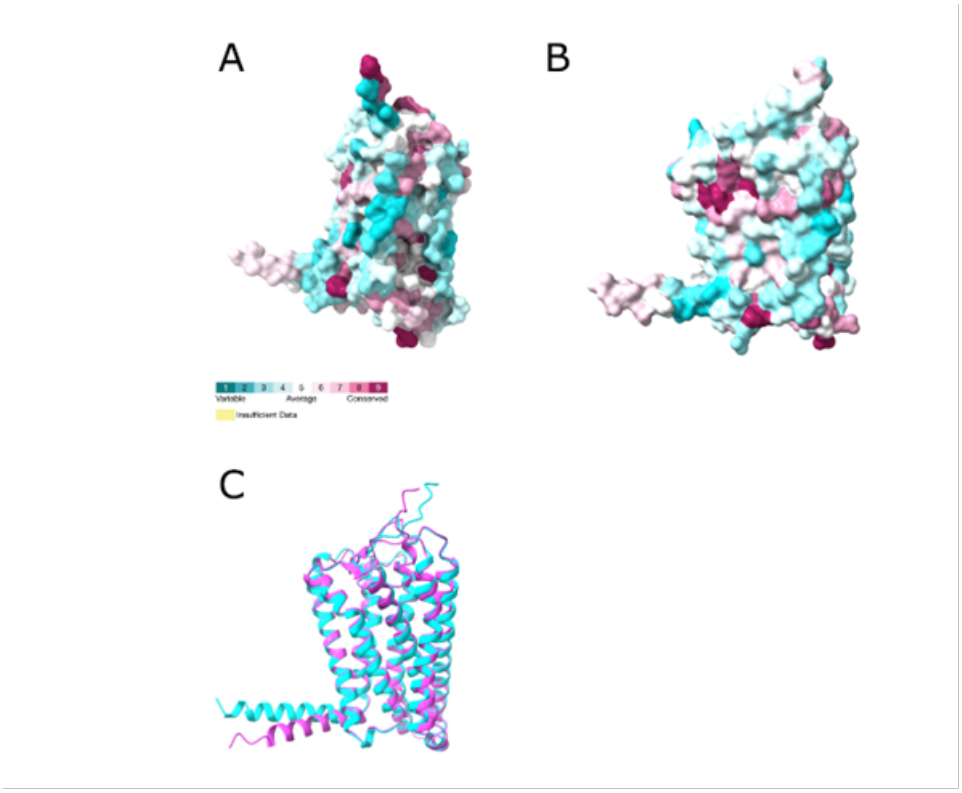


Figure 11: ConSurf analysis of predicted AlphaFold structures of Olfr691 and Olfr78 receptors.

A. ConSurf analysis of Olfr-691 AlphaFold structure (sequence from UniProt: Q3MI58). Conserved residues are dark red, and variable are light blue/green.

B. ConSurf analysis of Olfr-78 AlphaFold structure (sequence from UniProt: Q8VBV9). Conserved residues are dark red, and variable are light blue/green.

C. Overlap of Olfr-691 (magenta) and 78 (cyan) protein backbones

Additional experiments are needed for both receptors to further validate their oligomeric state in the basal and activated state as only one to two experiments were performed on each receptor. Furthermore, the use of other FFTs, such as FIF, when analyzing these receptors would be ideal to better quantify the concentrations of the different oligomeric states observed. While little is known about both Olfr78 and Olfr691, the significance of these receptors location in the renal system is not only significant, but also demonstrates the importance of continuing to promote research into orphaned GPCRs. The use of FFTs to ascertain the oligomeric status of proteins remains fundamental in molecular biology and biomedical research. The ability to investigate structural changes due to protein-ligand interactions broadens the pathway towards pharmaceutical success. Because of the advantages SpIDA encompasses over other FFTs, the gateway for research is significantly increased.

# REFERENCES


Ashkenazy H., Abadi S., Martz E., Chay O., Mayrose I., Pupko T., and Ben-Tal N. (2016). ConSurf 2016: An Improved Methodology to Estimate and Visualize Evolutionary Conservation in Macromolecules. *Nucl. Acids Res.* 2016; DOI: 10.1093/nar/gkw408

Barbeau A., Swift J., Godin A., De Koninck Y., Wiseman P., et al. (2013). Spatial intensity distribution analysis (SpIDA): a new tool for receptor tyrosine kinase activation and transactivation quantification. *Methods in Cell Biology* 117 1-19

Calebiro D. and Koszegi Z. (2019). The subcellular dynamics of GPCR signaling. *Molecular and Cellular Endocrinology* - in press. https://doi.org/10.1016/j.mce.2018.12.020

Congreve, M., Graaf, de C., Swain, A. Nigel, & Tate, A. Christopher. (2020). Impact of GPCR Structures on Drug Discovery. 181(1), 81–91. https://doi.org/10.1016/j.cell.2020.03.003

de Mendoza A, Sebé-Pedrós A, Ruiz-Trillo I. (2014). The evolution of the GPCR signaling system in eukaryotes: modularity, conservation, and the transition to metazoan multicellularity. *Genome Biol Evol*. doi: 10.1093/gbe/evu038

Fredriksson R., Lagerstrom M., Lundin L., Schioth H. (2003). The G-Protein-Coupled Receptors in the Human Genome Form Five Main Families. Phylogenetic Analysis, Paralogon Groups, and Fingerprint. *Molecular Pharmacology* 63 (6), 1256-1272

Gahbauer, Stefan, & Böckmann, Rainer A. (2016). Membrane-Mediated Oligomerization of G Protein Coupled Receptors and Its Implications for GPCR Function. *Frontiers in Physiology*. https://doi.org/10.3389/fphys.2016.00494

Godin, Antonio, G., Costantino, Santiago, Lorenzo, Louis-Etienne, & et al. (2011). “Revealing protein oligomerization and densities in situ using spatial intensity

distribution analysis". *PNAS*, 108(17), 7010–7015. https://doi.org/10.1073/pnas.1018658108

Harikumar K., Pinon D., Miller L. Transmembrane segment IV contributes a functionally important interface for oligomerization of the Class II G protein-coupled secretin receptor (2007) *Journal of Biological Chemistry* 282 (42) 30363-72.

Hashimoto, Kosuke, & Panchenko, Anna R. (2010). Mechanisms of protein oligomerization, the critical role of insertions and deletions in maintaining different oligomeric states. *Proceedings of the National Academy of Sciences*, 107(47). https://doi.org/10.1073/pnas.1012999107

Huang, Bo, Perroud, Thomas D., & Zare, Richard, N. (2004). Photon Counting Histogram: One-Photon Excitation. *ChemPhysChem*, 5, 1523–1531. https://doi.org/DOI: 10.1002/cphc.200400176

Jenkins, A.D., Kratochvíl, P., Stepto, R.F.T., & Suter, U.W. (1996). Glossary of basic terms in polymer science (IUPAC Recommendations 1996). *Pure and Applied Chemistry*, 68, 2287–2311. https://doi.org/10.1351/pac199668122287

Landau M., Mayrose I., Rosenberg Y., Glaser F., Martz E., Pupko T. and Ben-Tal N. (2005). ConSurf 2005: the projection of evolutionary conservation scores of residues on protein structures. *Nucl. Acids Res.* 33:W299-W302.

Oh, June. (2018). System-Wide Expression and Function of Olfactory Receptors in Mammals. *Genomics and Informatics*, 16(1). https://doi.org/10.5808/GI.2018.16.1.2

Pediani, John D., Ward, Richard J., Marsango, Sara, & Milligan, Graeme. (2018). Spatial Intensity Distribution Analysis: Studies of G Protein-Coupled Receptor Oligomerisation.

*Trends in Pharmacological Sciences*, 39(2), 175–186. https://doi.org/10.1016/j.tips.2017.09.001.

Poll, G. Brian, Chen, Lihe, & Chou, Chung-Lin., et al. (2021). Landscape of GPCR expression along the mouse nephron. *Am J Physiol Renal Physiol*, *321*, 50–68. https://doi.org/10.1152/ajprenal.00077.2021

Pluznick, Jennifer, Protzko, Ryan J., Peterlin, Zita, & et al. (n.d.). Olfactory receptor responding to gut microbiota-derived signals plays a role in renin secretion and blood pressure regulation. *Proceedings of the National Academy of Sciences*, 110(11), 4410–4415. https://www.pnas.org/doi/abs/10.1073/pnas.1215927110

Pull, Brian G., Xu, Jiaojiao, Gupta , Kunal, Tyler B. L. Pluznick, et al. (2021). Olfactory receptor 78 modulates renin but not baseline blood pressure. *Physiological Reports*, 1–10. https://doi.org/DOI: 10.14814/phy2.15017

Rajkumar, Premraj, Aisenberg, William, H., Acres, Aisenberg, W., Protzko, Ryan J., & Pluznick, Jennifer L. (n.d.). Identification and Characterization of Novel Renal Sensory Receptors. *PLoS ONE*, 9(10). https://doi:10.1371/journal.pone.0111053

Shepard BD, Natarajan N, Protzko RJ, Acres OW, Pluznick JL (2013) A Cleavable N-Terminal Signal Peptide Promotes Widespread Olfactory Receptor Surface Expression in HEK293T Cells. *PLoS ONE* 8(7): e68758. hhttps://doi:10.1371/journal.pone.0068758

Ward, Richard J., Marsango, S., Pediani, J.D., Milligan, G. (2017). The Use of Spatial Intensity Distribution Analysis to Examine G Protein-Coupled Receptor Oligomerization. In: Herrick-Davis, K., Milligan, G., Di Giovanni, G. (eds) G-Protein-Coupled Receptor Dimers. The Receptors, vol 33. *Humana Press, Cham*. https://doi.org/10.1007/978-3-319-60174-8_2

Ward, Richard J., Pediani, Godin G., Godin, Antonio, G., & Milligan, Graeme. (2015). Regulation of Oligomeric Organization of the Serotonin 5-Hydroxytryptamine 2C (5-HT2C) Receptor Observed by Spatial Intensity Distribution Analysis. *Journal of Biological Chemistry*, 290(20), 12844–12857. https://doi.org/DOI:https://doi.org/10.1074/jbc.M115.644724